Eur Radiol (2015) 25:800–811
DOI 10.1007/s00330-014-3463-8

PEDIATRIC

γ-H2AX foci as in vivo effect biomarker in children emphasize the importance to minimize x-ray doses in paediatric CT imaging

C. Vandevoorde · C. Franck · K. Bacher · L. Breysem · M. H. Smet · C. Ernst · A. De Backer · K. Van De Moortele · P. Smeets · H. Thierens

Received: 31 March 2014 / Revised: 16 September 2014 / Accepted: 1 October 2014 / Published online: 30 October 2014

Abstract
Objectives Investigation of DNA damage induced by CT x-rays in paediatric patients versus patient dose in a multicentre setting.
Methods From 51 paediatric patients (median age, 3.8 years) who underwent an abdomen or chest CT examination in one of the five participating radiology departments, blood samples were taken before and shortly after the examination. DNA damage was estimated by scoring γ-H2AX foci in peripheral blood T lymphocytes. Patient-specific organ and tissue doses were calculated with a validated Monte Carlo program. Individual lifetime attributable risks (LAR) for cancer incidence and mortality were estimated according to the BEIR VII risk models.
Results Despite the low CT doses, a median increase of 0.13 γ-H2AX foci/cell was observed. Plotting the induced γ-H2AX foci versus blood dose indicated a low-dose hypersensitivity, supported also by an in vitro dose–response study. Differences in dose levels between radiology centres were reflected in differences in DNA damage. LAR of cancer mortality for the paediatric chest CT and abdomen CT cohort was 0.08 and 0.13‰ respectively.
Conclusion CT x-rays induce DNA damage in paediatric patients even at low doses and the level of DNA damage is reduced by application of more effective CT dose reduction techniques and paediatric protocols.
Key Points
- *CT induces a small, significant number of double-strand DNA breaks in children.*
- *More effective CT dose reduction results in less DNA damage.*
- *Risk estimates based on the LNT hypothesis may represent underestimates.*

Keywords X-ray computed tomography · Double-strand DNA breaks · Radiobiology · gammaH2AX protein · Paediatrics

Abbreviations and acronyms

ATM	automatic tube current modulation
BEIR	biological effects of ionizing radiation
$CTDI_{vol}$	computed tomography dose index (volume)
DAPI	4′,6-diamidino-2-phenylindole
DNA	deoxyribonucleoside acid
DLP	dose–length product
DRL	dose reference level
DSB	double-strand break
γH2AX	phosphorylated histone subtype H2A isoform X

C. Vandevoorde (✉) · C. Franck · K. Bacher · H. Thierens
Department of Basic Medical Sciences, Ghent University, Proeftuinstraat 86, 9000 Gent, Belgium
e-mail: charlot.vandevoorde@ugent.be

L. Breysem · M. H. Smet
Radiology Department, University Hospital Louvain, Leuven, Belgium

C. Ernst
Radiology Department, University Hospital Brussels, Brussels, Belgium

A. De Backer
Radiology Department, General Hospital Sint-Lucas Ghent, Ghent, Belgium

K. Van De Moortele
5Radiology Department, General Hospital Sint-Jan Bruges, Bruges, Belgium

P. Smeets
Radiology Department, Ghent University Hospital, Ghent, Belgium

ICRP	International Commission on Radiological Protection
LAR	lifetime attributable risk
LNT	linear-no-threshold
LSS	lifespan study
53 PB1	p53 binding protein 1
PFA	paraformaldehyde
RAM-TRITC	rabbit-anti-mouse tetramethyl rhodamine isothiocyanate
RPMI	Roswell Park Memorial Institute

Introduction

The introduction of computed tomography (CT) has tremendously improved diagnostic imaging. However, the high x-ray doses associated with CT procedures have raised health concerns [1]. This is of particular importance for the paediatric patient population, recognized as one of the most important target groups in medical radiation protection. Technological developments in CT have substantially increased diagnostic applications and accuracy in paediatric patients. Children have a higher radiosensitivity compared to adults regarding x-ray-induced malignancies and the associated risk for exposure-induced death [2]. Therefore, optimisation and justification of CT protocols for children is a topic of high importance in daily clinical practice [3]. An initiative worth mentioning in this context is the Image Gently campaign of the Alliance for Radiation Safety in Paediatric Imaging, which tries to change practice by increasing awareness of the opportunities to reduce radiation dose in the imaging of children [4]. Several studies have shown that the use of CT dose reduction techniques in paediatric CT imaging lowers the physical radiation dose [5, 6]. However it remains unexplored if they also have an impact on the DNA damage induced by CT x-rays in children.

A recent study in the UK linked the exposure from x-rays in CT imaging during childhood to the development of brain tumours and leukaemia [7]. However, the risk assessments at low doses remain subject of active debate. The lifespan study (LSS) of atomic bomb survivors showed a roughly linear relationship between cancer mortality and high doses of high dose rate radiation for an adult population [8]. This resulted in the linear-no-threshold (LNT) hypothesis, implying a linear relationship between dose and biological effect without a dose threshold. Despite the considerable uncertainties and divergent views regarding the health effects and applicability of the LNT theory at low doses, the model is used for risk estimation by the international radiation protection community and referred to as the main paradigm of radiation protection [9].

The use of sensitive biomarkers for the assessment of early x-ray effects in patients gives valuable information on dose–effect relationships for diagnostic x-rays. Earlier work demonstrated that the γ-H2AX foci assay can be used to determine the effects of CT exposure at the molecular level, namely the induction of DNA double-strand breaks (DSBs) [10–13]. DSBs are considered to be the most deleterious cellular effects of x-rays, because they can result in loss or rearrangement of genetic information, leading to cell death or carcinogenesis [14]. The phosphorylation of the histone variant H2AX is one of the earliest stages in the cellular response to DSBs and one γ-H2AX focus represents one DNA DSB, which can be quantified by immunofluorescence microscopy [15].

A prospective multicentre study was set up in order to determine the number of x-ray-induced DNA DSBs in children undergoing a chest or abdomen CT examination. Herein, the γ-H2AX foci assay was used as an effect biomarker for radiation-induced DSBs. Blood doses were determined by a patient-specific full Monte Carlo dose simulation in order to correlate the induced DNA damage with the individual blood dose. BEIR VII age- and gender-specific risk models were used to assess the lifetime attributable risk (LAR) of cancer incidence and mortality associated with the CT examination of every individual patient.

Materials and methods

Assessment of DNA DSBs in pre- and post-CT blood samples of paediatric patients

Study population

The study population consisted of 51 children undergoing a CT examination of the chest (41) or abdomen (10) in one of the five participating radiology centres (March 2012 through July 2013) (Table 1). The small number of abdomen CT patients was because magnetic resonance imaging (MRI) was the preferred imaging modality of the majority of participating radiologists for abdomen investigations, to avoid ionizing radiation exposure. Exclusion criteria were present or past leukaemia or lymphoma and radiochemotherapy within the last year. The median age of the patient group was 3.8 years

Table 1 Demographic data of the paediatric patients included in the study

	Chest CT	Abdomen CT
Age (years)	3.00 (0.10–12.20)	7.1 (1.80–12.10)
Weight (kg)	13.50 (2.40–40.00)	24.00 (8.80–68.50)
Length (cm)	93.50 (45.50–160.00)	123.50 (76.50–167.00)
Men	30	7
Women	11	3

(range 0.1–12.5 years). Before blood sampling, an informed consent was signed by one of the parents of the children. The prospective multicentre study was approved by the local review boards of the participating hospitals, and the institutional review board of Ghent University Hospital acted as central ethical committee.

CT equipment and acquisition protocols

All the participating radiology departments used contemporary state-of-the-art low dose CT systems. The following CT systems were used in this study: Siemens Somatom Definition Flash and Sensation 64 (Siemens Medical Solutions, Germany), Toshiba Aquilion (Toshiba Medical Systems, Japan) and three centres used the GE Discovery CT750 HD (GE Healthcare, USA). Every radiology department used its own, optimized paediatric CT protocol with low kVp settings (median values: chest CT 80 kV, range 80–120 kV; abdomen CT 100 kV, range 100–120 kV), low fixed tube currents or automatic tube current modulation (ATM), adapted pitch values and imaging lengths restricted to the region of interest. Iterative reconstruction technology was applied in two of the institutions, resulting in ultra-low doses (VEO reconstruction from GE Healthcare). Individual CT parameters for the patients of the study are presented in Tables 2 and 3 for chest CT and abdomen CT respectively. The combination of state-of-the-art CT systems with dose reduction techniques and adapted paediatric protocols resulted in low- or even ultra-low CT doses.

Sample collection

Blood samples (2 mL) were collected through the catheter for contrast agent administration. One blood sample was taken before CT, to determine the baseline level of DSBs, and one approximately 5 min after the examination (the catheter was always flushed before sampling). As a result of occlusion, blood sampling through the catheter was not possible for more than half of the patients, especially very young children. For these patients an additional venepuncture after the CT exam was necessary. The blood samples were kept at 37 °C for 30 min to allow DNA damage signalling. Afterwards, DNA repair was arrested by cooling the samples at 0 °C for 15 min. Blood was transported at 4 °C, with an elapsed time no longer than 3 h from collection to processing. Before processing, samples were coded allowing blind scoring later on.

Detection of DNA DSBs

The method is based on the phosphorylation of the histone variant H2AX after DSB formation and follows previously published protocols [11, 16, 17]. In order to be able to work with a homogeneous cell population, T lymphocytes were isolated from the blood with the RosetteSep human T cell enrichment cocktail (StemCell Technologies, France) and resuspended in complete RPMI cell culture medium (84 % RPMI-1640, 15 % foetal calf serum, 1 %L-glutamine, 50 U/mL penicillin and 50 μg/mL streptomycin; Life Technologies, Belgium). For immunofluorescence staining, 250 μL of the resuspended T lymphocytes was centrifuged onto poly-L-lysine-coated slides (VWR International, Belgium). The slides were fixed in 3 % paraformaldehyde (PFA) (Sigma-Aldrich, Belgium) for 20 min and stored overnight in 0.5 % PFA. Fixation should immobilize antigens while retaining the lymphocytes as close to their natural state as possible. The next day, slides were permeabilised by dropping 100 μL of 0.2 % Triton-X-100 (Sigma-Aldrich, Belgium). This permeabilisation step is required because the anti-γ-H2AX antibody binding requires intracellular access to detect the γ-H2AX protein. The immunofluorescence staining was performed with an unlabelled primary mouse monoclonal anti-γ-H2AX antibody (1:500; Biolegend, Belgium) which specifically binds to the target γ-H2AX protein, followed by a secondary rabbit anti-mouse (RAM)–TRITC antibody (1:1,000; DakoCytomation, Denmark). This secondary antibody carries the (TRITC) fluorophore, recognizes the primary anti-γ-H2AX antibody and binds to it. Subsequently, the lymphocyte nucleus was counterstained with 2 % 4′,6-diamidino-2-phenylindole (DAPI) in Slowfade mounting medium (Sigma-Aldrich, Belgium). DAPI is a blue fluorescent stain specific for DNA. Microscopic scoring was performed manually with an Olympus BX60 fluorescence microscope with an Olympus×100/1.30 oil lens. The images were viewed using Cytovision software and captured with a digital camera (Applied Imaging, USA). Ten optical sections were obtained for each field of vision (Z-stack sections of 1.03 μm). Different images of one blinded slide were stored and on average 250 cells were scored manually for γ-H2AX foci. More than 250 cells were scored for every condition and the number of γ-H2AX foci induced by CT x-rays was obtained by subtracting the pre-scan foci yield from the post-scan foci yield after decoding. The scoring procedure was validated by double immunostaining for both γ-H2AX and p53 binding protein 1 (53BP1), to discriminate between background artefacts and small γ-H2AX foci. The experiments demonstrated that the γ-H2AX-TRITC foci coincide with 53BP1-FITC foci, resulting in a statistical significant agreement between the number of double stained foci (merge) and the number of individual γ-H2AX-TRITC foci (results not shown).

In vitro dose–response study on umbilical cord blood samples

For the validation of the in vivo results, a set of in vitro experiments was performed. Unfortunately, it was not possible to have access to blood samples with a larger volume than 2 mL from young children, because of ethical constraints.

Table 2 Individual CT parameters for all paediatric patients of the present study undergoing a chest CT examination

Patient number	Tube current (mA)	Exposure time (s)	Tube voltage (kV)	Pitch	Collimation (mm)	Type of CT scanner
1A	80	0.4	100	1.375	40	GE Discovery CT750 HD
1B*	60	0.4	100	1.375	40	GE Discovery CT750 HD
2	80	0.4	80	1.375	40	GE Discovery CT750 HD
3	35	0.6	100	1.375	40	GE Discovery CT750 HD (VEO)
4	30	0.4	100	0.984	40	GE Discovery CT750 HD
5	25	0.6	100	0.984	40	GE Discovery CT750 HD
6	38.3 (ATM)	0.5	80	1.375	40	GE Discovery CT750 HD
7	75	0.4	100	0.984	40	GE Discovery CT750 HD (VEO)
8	111.82 (ATM)	0.6	80	1.370	40	GE Discovery CT750 HD
9	86.86 (ATM)	0.6	80	1.375	40	GE Discovery CT750 HD
10	79	0.6	100	1.375	40	GE Discovery CT750 HD
11	94.98 (ATM)	0.6	120	1.375	40	GE Discovery CT750 HD
12	119.25 (ATM)	0.6	120	1.375	40	GE Discovery CT750 HD
13	22.47 (ATM)	0.4	80	0.516	40	GE Discovery CT750 HD (VEO)
14	22.58 (ATM)	0.4	80	0.516	40	GE Discovery CT750 HD (VEO)
15	18.90 (ATM)	0.4	80	0.516	40	GE Discovery CT750 HD (VEO)
16	31.54 (ATM)	0.4	80	0.516	40	GE Discovery CT750 HD (VEO)
17	10	0.4	80	0.984	40	GE Discovery CT750 HD (VEO)
18	41.42 (ATM)	0.4	80	0.984	40	GE Discovery CT750 HD (VEO)
19	19.66	0.4	80	0.516	40	GE Discovery CT750 HD (VEO)
20	61.69 (ATM)	0.4	80	0.516	40	GE Discovery CT750 HD (VEO)
21	24	0.4	80	0.516	40	GE Discovery CT750 HD (VEO)
22	37.67	0.4	80	0.516	40	GE Discovery CT750 HD (VEO)
23	39.15 (ATM)	0.4	80	0.516	40	GE Discovery CT750 HD (VEO)
24	31.13	0.4	80	0.516	40	GE Discovery CT750 HD (VEO)
25	10	0.4	80	0.984	40	GE Discovery CT750 HD (VEO)
26	35.84 (ATM)	0.4	80	0.516	40	GE Discovery CT750 HD (VEO)
27	21.58	0.4	80	0.516	40	GE Discovery CT750 HD (VEO)
28	29.81 (ATM)	0.4	80	0.516	40	GE Discovery CT750 HD (VEO)
29	33.30 (ATM)	0.4	80	0.516	40	GE Discovery CT750 HD (VEO)
30	122.32 (ATM)	0.285	120	0.900	38.4	Siemens Somatom Definition Flash
31	73.28 (ATM)	0.5	100	1.400	38.4	Siemens Somatom Definition Flash
32	163.19 (ATM)	0.5	100	1.200	38.4	Siemens Somatom Sensation 64
33	63.42 (ATM)	0.5	100	1.400	38.4	Siemens Somatom Definition Flash
34	124.31 (ATM)	0.5	100	1.400	38.4	Siemens Somatom Definition Flash
35	48.31 (ATM)	0.5	100	1.200	38.4	Siemens Somatom Definition Flash
36	160.54 (ATM)	0.5	100	1.200	38.4	Siemens Somatom Definition Flash
37	127.81 (ATM)	0.5	100	1.200	38.4	Siemens Somatom Definition Flash
38	89.89 (ATM)	0.5	100	1.200	38.4	Siemens Somatom Definition Flash
39	77.12 (ATM)	0.5	100	1.200	38.4	Siemens Somatom Definition Flash
40	157.67 (ATM)	0.5	80	1.200	38.4	Siemens Somatom Definition Flash
41	138.39 (ATM)	0.5	80	1.200	38.4	Siemens Somatom Definition Flash

ATM automatic tube current modulation, *VEO* iterative reconstruction

* Problems with contrast agent administration

Since umbilical cord blood is physiologically and genetically part of the foetus, we can consider this as blood of a newborn [18]. Therefore, umbilical cord blood samples were irradiated in vitro in order to compare the γ-H2AX foci dose response

Table 3 Individual CT parameters for all paediatric patients of the present study undergoing an abdomen CT examination

Patient number	Tube current (mA)	Exposure time (s)	Tube voltage (kV)	Pitch	Collimation (mm)	Type of CT scanner
1	70.5	0.6	100	1.375	40	GE Discovery CT750 HD
2	325	0.8	100	0.984	40	GE Discovery CT750 HD
3	120	0.5	100	0.844	32	Toshiba Aquilion
4A	188.63 (ATM)	0.5	120	0.900	38.4	Siemens Somatom Definition Flash
4B*	349.5 (ATM)	0.285	100	0.600	38.4	Siemens Somatom Definition Flash
5	184.21 (ATM)	0.5	100	0.900	38.4	Siemens Somatom Definition Flash
6A	49.7 (ATM)	0.5	100	1.200	38.4	Siemens Somatom Definition Flash
6B*	47.38 (ATM)	0.5	100	1.200	38.4	Siemens Somatom Definition Flash
7	152.32 (ATM)	0.5	100	1.200	38.4	Siemens Somatom Definition Flash
8	105.69 (ATM)	0.5	100	1.400	38.4	Siemens Somatom Definition Flash
9	122.55 (ATM)	0.5	100	1.400	38.4	Siemens Somatom Definition Flash
10	75.92 (ATM)	0.5	100	1.200	38.4	Siemens Somatom Definition Flash

ATM automatic tube current modulation

* One scan with and one scan without contrast agent administration

after in vivo and in vitro exposure. Cord blood samples from three healthy donors were exposed to 1, 2, 4, 6, 8, 10, 15, 20 and 500 mGy and one blood sample was sham-irradiated. A radiation quality of 100-kVp x-rays and 2-mm Al filtration was used, with a Philips MG420 x-ray generator coupled to an MCN420 tube. The irradiation was carried out in a 37 °C water bath. Calibration was performed with an NE2571 Farmer ionization chamber (Thermo Electron, Altrincham, UK). The irradiated blood samples were kept for 30 min at 37 °C, followed by 15 min on ice water to simulate the situation of patient blood samples after in vivo exposure. The same γ-H2AX foci protocol and scoring method as described for the in vivo study was applied. The use of cord blood for in vitro experiments was approved by the institutional review board.

Patient dosimetry

Calculation of blood and organ doses induced by CT x-rays by full Monte Carlo simulation

The blood dose was calculated as a weighted sum of doses to the largest blood-containing organs with the percentage of blood pool as weighting factor, namely lungs (12.5 %), heart (10 %), liver (10 %) and remainder (67.5 %) [19]. In order to obtain individual organ dose estimates, an individualized full Monte Carlo patient dose simulation was set up using ImpactMC simulation software 1.3.1 (CT Imaging GmbH, Germany). In this software, patient-specific 3D voxel models are created on the basis of the CT images acquired during CT examination [20]. For the simulation of the CT scan, actual scan parameters, such as tube voltage (kV), tube current–exposure time product (mAs) and pitch, are retrieved from the DICOM header of the CT images. The individual mA values of all the reconstructed CT slices were used in order to take into account of the tube current modulation of the CT scanner. More than 10^{10} photons were simulated in order to minimize the uncertainty in the Monte Carlo results. The patient-specific dose distribution was determined by multiplying the air kerma normalized dose distribution from the simulations with the actual air kerma value (mGy) measured free-in-air in the isocentre of the scanner by using a pencil ionization chamber (RaySafe Xi CT detector, Unfors RaySafe, Sweden). In addition to the organ doses needed for the blood dose evaluation, doses to other organs and tissues of interest according to the BEIR VII risk models were also calculated with this Monte Carlo patient dose simulation. Organ volumes were segmented in the original CT images and organ dose deposition was calculated on the basis of the Monte Carlo dose distribution. For the bone marrow, all bony structures in the field of view were segmented and the bone marrow dose was calculated as the weighted sum of the doses to these structures with the percentage of bone marrow in these compartments as weighting factor [21]. To account for differences in photon absorption in bone and bone marrow, the obtained value was corrected for the ratio of mass absorption coefficients in soft tissue and bone [22].

Calculation of effective dose

To compare the dose levels of the CT procedures in the current study with similar procedures in different hospitals and countries, the effective dose was calculated for the total group of chest CT and abdomen CT patients. Effective dose is a quantity reflecting the stochastic risk associated with an exposure to ionizing radiation at a population level. The effective doses of the paediatric populations under study were derived from

the individual DLP values by using the conversion factors published by Deak et al. as function of kVp, imaging region and age for ICRP publication 103 recommendations [23].

Risk estimation

Individual LAR of cancer incidence and mortality related to a chest or abdomen CT scan were calculated according to the BEIR VII risk models for different cancer types, taking into account age-dependent incidence and mortality rates within the Euro-American population [24]. Input for these risk assessments was the simulated organ doses and the age of the individual patients. The LAR data from BEIR VII were adapted for a dose and dose-rate effectiveness factor of 2 as proposed by the ICRP [25].

Statistical analysis

Statistical analysis was performed with Microsoft Office Excel 2010 (Microsoft Corporation, USA) and Statistical Package for Social Sciences software version 22 (SPSS Inc., USA). Poisson statistics were applied to calculate the statistical accuracy of the number of x-ray induced γ-H2AX foci. The differences between the pre- and post-CT data sets were evaluated for significance with the paired sample Wilcoxon signed-rank test (95 % confidence level). Linear regression analysis was applied to evaluate age dependence. A p value less than 0.05 was considered as statistically significant.

Results

Assessment of DNA DSBs in pre- and post-CT blood samples of paediatric patients

An increase in DNA DSBs was observed for every patient, except for one chest CT patient with a very low blood dose of 0.14 mGy. The median pre-exposure level was 0.56 foci/cell (range 0.23–1.20 foci/cell) and the post-exposure level was 0.72 foci/cell (range 0.31–1.44 foci/cell). The pre- and post-CT exposure foci levels are presented in Fig. 1 for every individual patient. The median number of induced foci representing DNA DSBs induced by CT was 0.13 foci/cell (range −0.07 to 0.49 foci/cell) and the median blood dose 0.94 mGy (range 0.14–8.85 mGy). The present study shows that nearly every CT procedure induces DNA DSBs in T lymphocytes of paediatric patients. A Wilcoxon signed-rank test showed a statistically significant difference in the mean level of DNA DSBs pre-CT and the mean level post-CT per patient ($p<0.001$). Moreover, the number of induced DSBs is strongly blood dose dependent as illustrated in Fig. 2.

To investigate the intrinsic higher radiosensitivity of children decreasing with age, the number of induced γ-H2AX foci was divided by the calculated blood dose and plotted versus age of the paediatric patient. The linear fit in Fig. 3 indicates a diminishing trend of the foci-to-dose ratio versus age; however, regression analysis showed that the decrease of the foci-to-dose ratio versus age was not statistically significant ($p=0.204$).

In vitro dose–response study on umbilical cord blood samples

The results of the in vitro irradiation of umbilical cord blood, repeated for three different donors, are also presented in Fig. 2. The in vivo and in vitro dose–response curves show both an initial sharp increase with dose and appear not linear at all. The dashed line in Fig. 2 represents an extrapolation according to the LNT hypothesis of the in vitro dose response of γ-H2AX foci in cord blood at doses (5.68 γ-H2AX foci/cell for 0.5 Gy) higher than zero. This shows clearly that the foci numbers in the low dose range are much higher than expected from the LNT extrapolation of high dose behaviour.

Patient dosimetry

Monte Carlo calculations resulted in a median blood dose for chest CT patients of 0.86 mGy (0.14–2.84 mGy) and for abdomen CT patients of 1.62 mGy (0.66–8.85 mGy). The median effective dose value for the chest CT patient cohort was 1.14 mSv (range 0.17–3.10 mSv). For the abdomen CT patient cohort, the median effective dose value was higher, namely 2.82 mSv (range 1.18–10.55 mSv). A comparison of these values with literature data confirms that in the present study patient doses were low [26, 27]. All participating centres used state-of-the-art low dose equipment and specific paediatric protocols, resulting in very low $CTDI_{vol}$ and DLP values of the patients compared with the national dose reference levels (DRLs) (Table 4). Reference levels are typically set at the 75th percentile of the dose distribution from a conducted survey. The median $CTDI_{vol}$ and DLP values in the current study are below the 75th percentile values and close to the 25th percentile, which represents good clinical practice. However, substantial differences in dose-sparing equipment and imaging protocols for children resulted in differences in patient doses and corresponding DNA damage. Figure 4 shows a clear correlation between both parameters when comparing the data for the different participating hospitals. This figure emphasizes that the use of more powerful dose

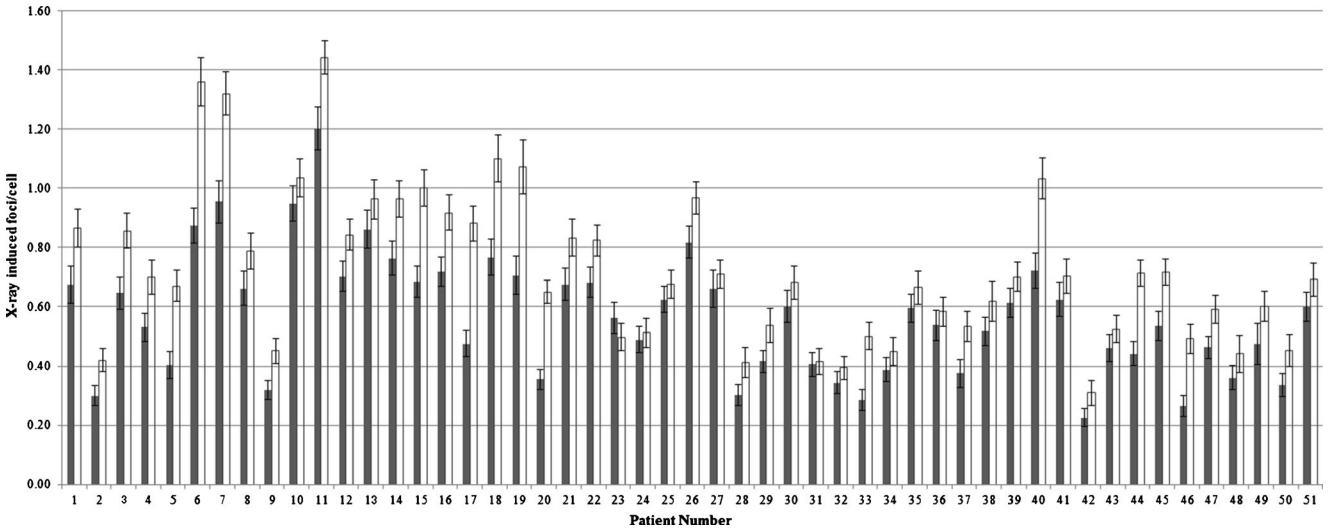

Fig. 1 Comparison of γ-H2AX-foci levels pre- and post-CT x-ray exposure for every individual patient of the study. *Error bars* represent standard deviations on foci yields calculated following Poisson statistics

reduction techniques and protocols involving a lower patient dose also results in less radiation effects for paediatric patients according to the DNA damage effect biomarker.

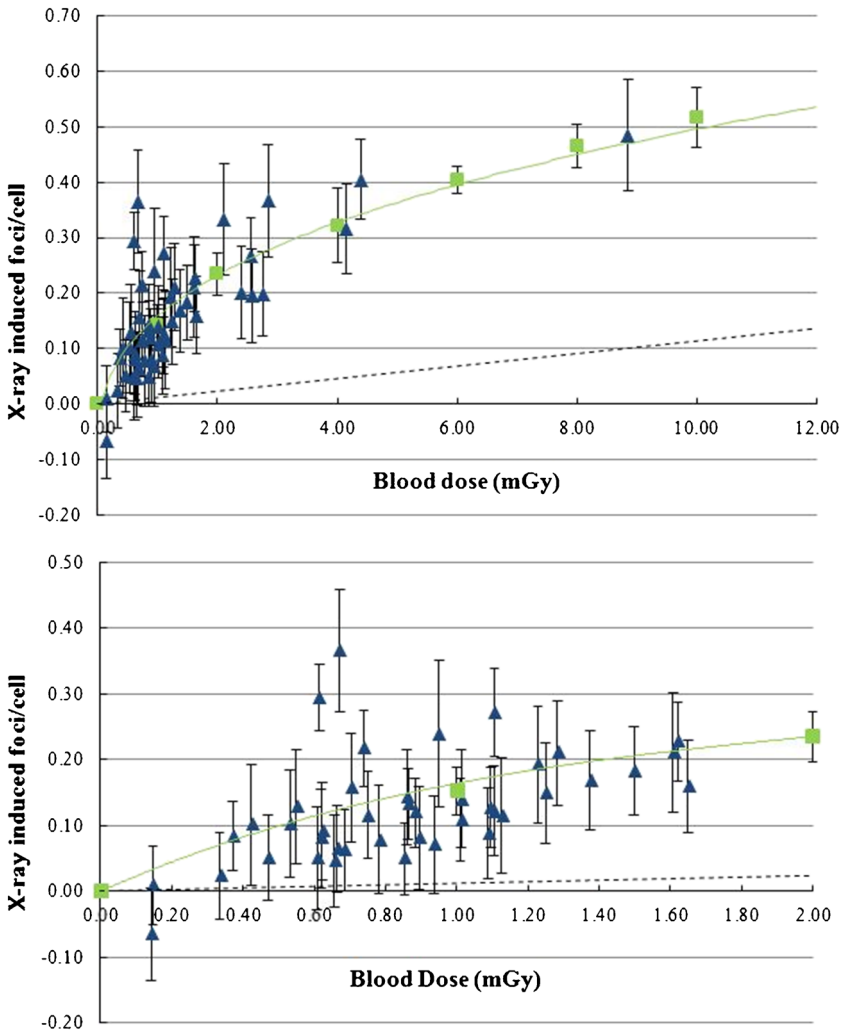

Fig. 2 **a** The mean number of γH2AX-foci per cell induced by in vivo x-ray exposure plotted versus the Monte Carlo calculated blood dose for every paediatric patient undergoing a chest CT or abdomen CT (in *blue*). The *whiskers* represent standard deviations derived from the statistical accuracy of the scored number of foci in the blood samples taken before and after CT examination (Poisson statistics). The dose–response curve after in vitro x-ray irradiation of cord blood is also shown (in *green*). The *whiskers* of the in vitro study represent SDs among the three different donors. The *dashed line* represents a linear extrapolation based on the γ-H2AX foci induced in cord blood after an in vitro dose of 0.5 Gy, based on the LNT hypothesis. Since a large part of the data are clustered in 0–2 mGy range, this range is presented as a separate figure (**b**)

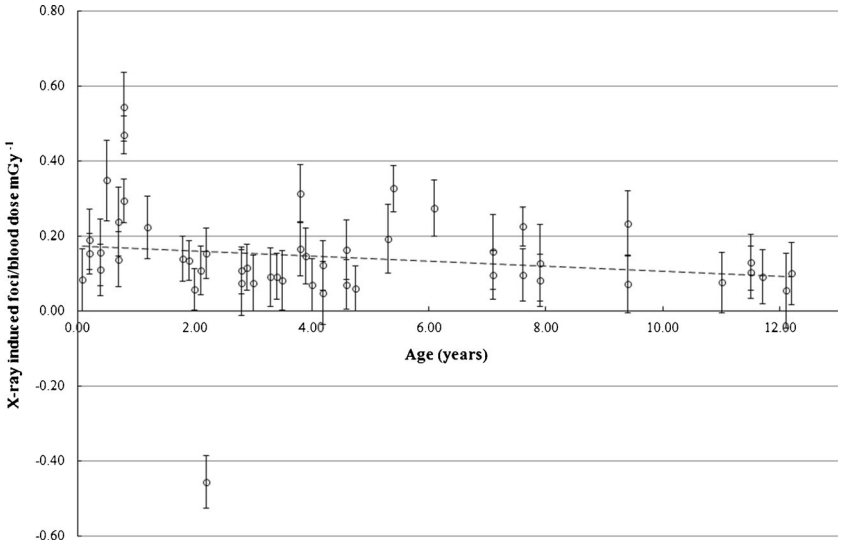

Fig. 3 The number of γ-H2AX foci normalized to blood dose, as a function of age of the paediatric patients. The *dashed line* is the result of a linear fit

Risk estimation

Based on the Monte Carlo calculated organ doses, individual LAR values for cancer incidence and mortality according to the BEIR VII risk models were calculated for every patient. The BEIR VII report provides a method to estimate LAR of cancer incidence and mortality based on the organ doses associated with the radiation exposure and a patient's age at the time of exposure. Table 5 represents the median LAR values of cancer incidence and mortality related to leukaemia and different types of solid cancer of organs in the field of view based on the simulated organ doses. The range of LAR values over the patient cohorts is indicated between brackets. For the total patient cohort undergoing a chest CT examination the LAR values for cancer incidence and mortality are respectively 0.17 per thousand and 0.08 per thousand. For the total group of paediatric patients undergoing an abdomen CT examination the LAR incidence and mortality are respectively 0.32 per thousand and 0.13 per thousand.

Table 4 Comparison of the median $CTDI_{vol}$ (mGy) and DLP (mGy cm) values of the chest CT and abdomen CT investigations in this study with the national DRLs (75th percentile) in Belgium. As an indication of good clinical practice, the 25th percentile is also presented

	Chest CT	Abdomen CT
$CTDI_{vol}$ (mGy)		
25th percentile	1.85	2.80
75th percentile (DRL)	5.00	6.75
Study data	1.54 (0.22–4.07)	4.17 (1.11–13.98)
DLP (mGy cm)		
25th percentile	40.00	100.00
75th percentile (DRL)	130.00	315.00
Study data	24.80 (4.57–130.36)	315 (33.00–698.82)

Discussion

Our study provides evidence that CT induces DNA damage in paediatric patients, even at low doses (blood doses in the range of 0.15–8.85 mGy). Several studies reported γ-H2AX foci induction by CT x-ray exposure in adult patients [10–13, 28]. However none of them investigated the DNA damage induced by CT radiation exposure in paediatric patients, nor the ultra-low dose region evaluated in the current study. Stephan et al. conducted a small scale pilot study with blood samples from ten paediatric patients undergoing CT examinations, in which chromosome analysis in lymphocytes showed a significant increase in dicentric frequencies and excess acentric fragments [29]. However, the mean blood dose of the cohort of ten children in that study was 12.9 mGy compared to the low mean blood dose of 1.35 mGy for the 51 patients in the current study.

Currently, the vast majority of publications use the concept of effective dose to assess CT radiation burden. However, effective dose calculations can never be linked to an individual patient exposure, as reference phantoms need to be used and the quantity effective dose is designed for risk estimation in a population. To interpret the in vivo γ-H2AX foci data, it is very important to have an accurate blood dose calculation for every patient, which takes into account the patient's anatomy, different types of CT systems, dose reduction technologies and various types of CT protocols. However, the latter analysis cannot be performed by using effective dose. This was accomplished by a Monte Carlo simulation of radiation transport in patient-specific 3D voxel models derived from the CT images. For dosimetry of paediatric patients the use of voxel models is a substantial improvement compared to dose calculation based on anthropomorphic paediatric standard phantoms, as the full Monte Carlo simulation takes into account the real anatomy of the patient.

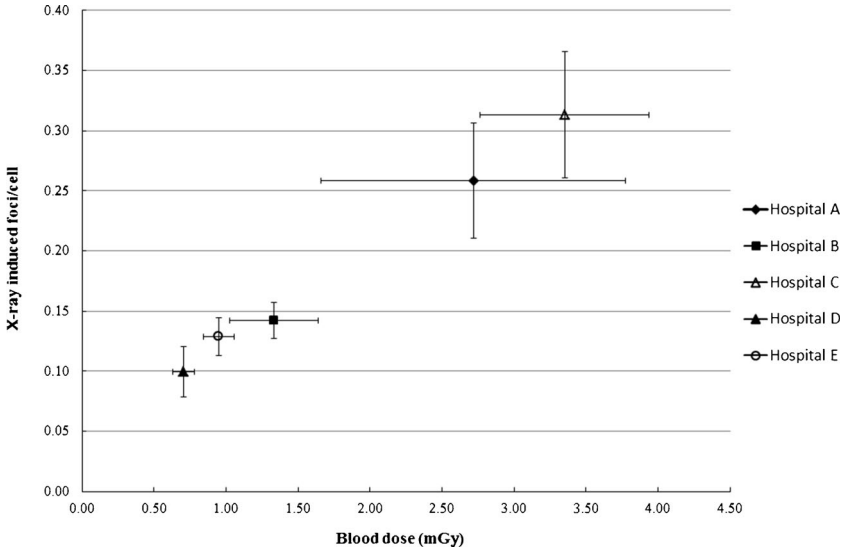

Fig. 4 The mean γ-H2AX foci per cell induced by CT x-rays plotted against the mean patient blood dose for participating centres. The CT equipment used by the participating centres was as follows: hospital A, GE Discovery CT750 HD; hospital B, GE Discovery CT750 HD (VEO); hospital C, Siemens Somatom Definition Flash and Toshiba Aquilion; hospital D, GE Discovery CT750 HD (VEO); hospital E, Siemens Somatom Definition Flash and Sensation 64. *Whiskers* represent the standard deviation on the mean of foci numbers and blood doses

Table 5 LAR of cancer incidence and mortality, according to the BEIR VII model, associated with x-ray exposure from chest CT and abdomen CT examinations for the cohort of paediatric patients included in the study

	$LAR_{incidence}$ (‰)	$LAR_{mortality}$ (‰)	$LAR_{incidence}$ (‰)	$LAR_{mortality}$ (‰)
Chest CT				
	Men (30)		Women (11)	
Age (year)	3.20 (0.20–11.50)		2.00 (0.10–12.20)	
Blood dose (mGy)	0.81 (0.14–2.84)		0.86 (0.55–2.56)	
Stomach	0.007 (0.001–0.017)	0.004 (0.001–0.009)	0.011 (0.005–0.033)	0.006 (0.003–0.019)
Liver	0.005 (0.001–0.011)	0.003 (0.001–0.008)	0.002 (0.001–0.005)	0.002 (0.001–0.005)
Lung	0.034 (0.006–0.130)	0.035 (0.006–0.131)	0.088 (0.049–0.275)	0.077 (0.043–0.241)
Breast	–	–	0.159 (0.048–0.415)	0.037 (0.011–0.097)
Thyroid	0.011 (0.002–0.032)	–	0.078 (0.043–0.141)	–
Remainder	0.037 (0.005–0.094)	0.014 (0.002–0.034)	0.038 (0.020–0.146)	0.014 (0.008–0.055)
Leukaemia	0.002 (0.000–0.007)	0.001 (0.000–0.004)	0.002 (0.001–0.003)	0.001 (0.000–0.002)
All cancers	0.099 (0.015–0.287)	0.055 (0.009–0.184)	0.378 (0.171–1.016)	0.137 (0.067–0.417)
Abdomen CT				
	Men (7)		Women (3)	
Age (years)	7.10 (1.80–12.10)		7.90 (6.10–11.00)	
Blood dose (mGy)	1.61 (0.66–8.85)		1.38 (1.09–4.15)	
Stomach	0.018 (0.007–0.058)	0.009 (0.004–0.030)	0.010 (0.008–0.035)	0.006 (0.005–0.020)
Colon	0.089 (0.035–0.337)	0.043 (0.017–0.158)	0.045 (0.028–0.110)	0.021 (0.013–0.051)
Liver	0.014 (0.006–0.047)	0.010 (0.004–0.033)	0.005 (0.002–0.013)	0.004 (0.002–0.011)
Lung	0.018 (0.011–0.065)	0.018 (0.011–0.063)	0.067 (0.031–0.068)	0.059 (0.027–0.059)
Prostate	0.024 (0.004–0.075)	0.005 (0.001–0.032)	–	–
Uterus	–	–	0.008 (0.005–0.021)	0.002 (0.001–0.005)
Ovary	–	–	0.021 (0.009–0.042)	0.011 (0.005–0.023)
Bladder	0.054 (0.010–0.176)	0.012 (0.002–0.037)	0.039 (0.002–0.099)	0.011 (0.006–0.028)
Remainder	0.077 (0.015–0.274)	0.027 (0.005–0.096)	0.100 (0.029–0.273)	0.025 (0.012–0.071)
Leukaemia	0.008 (0.002–0.029)	0.003 (0.001–0.018)	0.005 (0.004–0.015)	0.002 (0.002–0.009)
All cancers	0.318 (0.091–1.047)	0.131 (0.046–0.445)	0.329 (0.263–0.677)	0.130 (0.108–0.277)

Values are median (range), based on the individual simulated organ doses and the age of the individual patients

In addition the results of the present study show that lower patient doses related to more effective CT dose reduction strategies for paediatric patients also result in a similar decrease in DNA DSBs as effect biomarker. It is internationally recognized that CT dose optimization is essential, especially for children taking into account not only dose reduction but also diagnostic image quality. A number of CT dose surveys showed substantial differences between practices for the same type of examination, suggesting that not all institutions have suitably optimized their CT protocols [30, 31]. Dose-saving strategies are continuously evolving in terms of imaging techniques as well as dose management, and the results of the present study stress the importance of dose reduction in paediatric CT imaging. As already shown by the values of the calculated blood doses and the comparison of DLP and $CTDI_{vol}$ values with national DRLs, paediatric CT radiation doses were substantially low in all participating radiology departments. One of the institutions (hospital D in Fig. 4) achieved very low doses (mean blood dose, 0.71 mGy) by using iterative reconstruction for all CT examinations; however, only chest CT patients were recruited in this institution. For the patient cohort of institution D, a very low mean level of induced γ-H2AX foci per cell (0.10 foci/cell) was recorded. Hospital E achieved a mean blood dose of 0.95 mGy corresponding to 0.13 induced foci/cell, and the data for this hospital are a mixture of chest CT and abdomen CT investigations. For both types of examination DLP values in this hospital were very low compared to the DRL (reported in Table 4). The median DLP value for abdomen CT patients in hospital E was 60.00 mGy cm (range 33.00–87.20 mGy cm), which is lower than the 25th percentile of 100 mGy cm.

When the number of induced γ-H2AX foci is plotted versus blood dose, the data point to a low-dose hypersensitivity. The observed low-dose hypersensitive response in paediatric CT is consistent with the data of a previous study on paediatric patients undergoing a cardiac catheterization [17]. The in vitro dose–response curve for umbilical cord blood shows the same behaviour in the low dose range and supports the in vivo results.

The observed low-dose hypersensitivity challenges the LNT hypothesis, assuming less DNA damage, and can be explained by the "bystander effect" [32]. Genetic/epigenetic changes occur not only in cells hit by the ionizing particles but also in non-irradiated cells that are neighbouring directly hit cells. The bystander effect amplifies the effects of radiation by increasing the number of affected cells, owing to cell–cell communication or soluble factors released by irradiated cells. Bystander effects are observed after co-cultivation of irradiated and non-irradiated cells and transfer of medium from irradiated to non-irradiated cells [33, 34]. For cells in direct contact, bystander signalling can occur through gap junction intercellular communication [35, 36]. A second route by which bystander responses are mediated is through the release of soluble factors from cells that have been irradiated. These factors have been extensively studied and several of these key molecules are central players involved in stress responses and cell–cell signalling, which are not generally specific to radiation exposure [35]. Moreover, many aspects of bystander-mediated response have close parallels to inflammatory responses. This was recently shown in a gene set enrichment analysis that highlighted different gene expression profiles in whole blood samples irradiated with low and high doses of x-rays. Functional analysis of genes differentially expressed at 0.05 Gy showed the enrichment of chemokine and cytokine signalling [37]. In a study by Mancuso et al., DNA damage, apoptosis and tumour induction were observed in the shielded cerebellum of mice heterozygous for *Patched* after partial-body irradiations [38]. This indicates that bystander effects in vivo have carcinogenic potential.

A possible confounder in the present study could be the increase in DSB levels due to the administration of contrast agent and the corresponding emission of secondary radiation in CT imaging. However, previous studies showed that there was no biological dose-enhancing effect if radiation and contrast agent are within the diagnostic range [11, 39].

Epidemiological data indicate a higher relative risk of cancer per unit of radiation dose for children compared to adults, and children have also a longer lifetime for radiation-related cancer to occur [2]. We observed a non-significant age dependency in our present study of x-ray-induced DNA DSBs. To study age dependence, the study population should be broadened and a more uniform distribution of the ages is required.

Using the calculated organ doses, the LAR for cancer mortality in the paediatric patient population undergoing a low dose chest or abdomen CT was of the order of 0.1‰ according to the BEIR VII data assuming the LNT hypothesis. The thyroid gland, breast tissue and gonads are structures that have an increased sensitivity to radiation in growing children. Some of these regions, such as thyroid and breast tissue, are routinely involved in chest CT imaging. Miglioretti et al. [27] calculated radiation exposure and LAR for cancer incidence from a random sample of paediatric CTs. Their calculated LARs are an order of magnitude higher than those reported in the current study: abdomen CT 1–4‰ versus 0.3‰ (median), chest CT 2–3‰ versus 0.1–0.4‰ (median boys–girls). The main reason for the lower risk estimates in the current study are lower patient doses compared to the work of Miglioretti et al. [27]. They reported a mean ED of 12.5 mSv for abdomen CT and 6.3 mSv for chest CT, whereas in the present work the median ED values were 2.8 mSv and 1.1 mSv respectively. The lower doses and corresponding risk estimates in the current work reflect the use of contemporary state-of-the-art low dose CT equipment and the successful implementation of dose reduction strategies for paediatric

CT imaging by the participating radiology departments (as illustrated in Table 4).

Large uncertainties are associated with the risk estimates summarized in Table 5. The BEIR VII committee estimates that the excess cancer mortality due to radiation can be estimated within a factor of 2 (at 95 % confidence level). For leukaemia the corresponding factor is 4. The LNT model applied by the BEIR VII committee is based mainly on epidemiological data for radiation-induced cancers in the atomic bomb survivors in the dose range of about 100 mSv to 2.5 Sv [8]. For lower doses involved in diagnostic radiology, epidemiological data are not available to support the LNT model mainly owing to the necessary sample size [40]. Application of the LNT hypothesis in the low dose range may lead to an overestimation of the risk in case of the existence of a dose threshold or an underestimate in case of cooperative multicellular radiation effects such as bystander effects. It is anticipated that significant insights into dose response and cancer risks in the low dose range will emerge from molecular epidemiology studies incorporating biomarkers and bioassays [41]. The low-dose hypersensitivity observed in the γ-H2AX foci dose response of the present study indicates that LAR estimates based on the LNT model may potentially underestimate the risks of paediatric CT imaging.

For conclusions with respect to the risk of stochastic effects of x-rays, the present study has limitations. Biological damage in T lymphocytes reflects only the damage in one tissue, namely the blood. However, we may assume that DNA damage and repair in peripheral blood lymphocytes are representative for other normal tissues [42]. Using the γ-H2AX foci assay, only DNA DSBs induced by CT x-rays are detected but not the outcome of the DNA repair process. DNA DSBs are considered to be particularly biologically important because their repair is more difficult than other types of DNA damage. Cells have evolved mechanisms to monitor genome integrity and they respond to DNA damage by activating a complex DNA damage response pathway. Erroneous repair of DNA DSBs can result in chromosomal rearrangements, including translocations, which are associated with tumorigenesis [43]. An increase in chromosomal aberrations due to a defect in DNA repair, as observed in ataxia-telangiectasia (AT) patients, leads to genetic instability, which in turn enhances the rate of cancer development [44]. In the framework of cancer risk, a direct assessment of mutations in DNA or chromosomal aberrations induced by CT x-rays in paediatric patients' lymphocytes would provide added value taking into account the mutagen–carcinogen link. However, this kind of study is not obvious in view of the low sensitivity of contemporary mutagenicity assays.

The present study emphasizes the need to optimize and minimize radiation exposure in paediatric CT imaging: lower patient doses entail less DNA damage in children. This implies the need for justification of the indications for which medical imaging involving ionizing radiation is used. From a patient's perspective, the benefits of a medically necessary CT scan far exceed the small radiation-induced cancer risk. However, some studies suggest that a third of paediatric CT scans are unnecessary [1]. This indicates that the referring physician and radiologist should consider whether the exam is truly clinically indicated and was not recently performed in another hospital. Furthermore, they should check if no alternative diagnostic procedure might be available, one not involving ionizing radiation such as ultrasound and MRI. When CT is indicated, great care should be taken to optimize radiation exposures in order to minimize the risk for carcinogenic effects later in life. Strategies to optimize radiation doses in paediatric CT imaging are adjustment of the CT parameters to the child's size (guidelines on individual size/weight parameters [45]), the scan length should be restricted to the region of interest and dose reduction techniques should be implemented taking into account the required image quality (ATM, iterative reconstruction and/or adaptive collimation). The observations of the present work should encourage medical practitioners to maximize the benefit-to-risk ratio of CT imaging in paediatric radiology.

Acknowledgments We wish to thank all patients and their parents who consented to participate in this study. We also express our gratitude to Hilde Vandenhout, Ilse Roebben and the nurses of the participating hospitals for their help with the collection of blood samples. A special thank you to Dr. Wim Decaluwe from the neonatology department at AZ Sint-Jan, Bruges, for his support and dedication to this study. Furthermore, we acknowledge the master thesis students for their help with processing of the blood samples. Above all, we would like to thank Iris Rossaert, Virginie De Gelder and Sofie De Langhe for their practical support. The study was financially supported by the Federal Agency of Nuclear Control, Belgium (CO-90-09-2329-00).

The scientific guarantor of this publication is Prof. Hubert Thierens. The authors of this manuscript declare no relationships with any companies whose products or services may be related to the subject matter of the article. No complex statistical methods were necessary for this paper. Institutional review board approval was obtained. Written informed consent was obtained from all subjects (patients) in this study. Methodology: prospective, experimental, multicenter study.

References

1. Brenner DJ, Hall EJ (2007) Current concepts - computed tomography - an increasing source of radiation exposure. N Engl J Med 357:2277–2284
2. UNSCEAR (2013) Sources, effects and risks of ionizing radiation. Report to the General Assembly of the United. Nations, New York
3. Nievelstein RAJ, van Dam IM, van der Molen AJ (2010) Multidetector CT in children: current concepts and dose reduction strategies. Pediatr Radiol 40:1324–1344

4. Strauss KJ, Goske MJ, Kaste SC et al (2010) Image gently: ten steps you can take to optimize image quality and lower CT dose for pediatric patients. Am J Roentgenol 194:868–873
5. Gay F, Pavia Y, Pierrat N, Lasalle S, Neuenschwander S, Brisse HJ (2014) Dose reduction with adaptive statistical iterative reconstruction for paediatric CT: phantom study and clinical experience on chest and abdomen CT. Eur Radiol 24:102–111
6. Brady SL, Moore BM, Yee BS, Kaufman RA (2014) Pediatric CT: implementation of ASIR for substantial radiation dose reduction while maintaining pre-ASIR image noise. Radiology 270:223–231
7. Pearce MS, Salotti JA, Little MP et al (2012) Radiation exposure from CT scans in childhood and subsequent risk of leukaemia and brain tumours: a retrospective cohort study. Lancet 380:499–505
8. Preston DL, Shimizu Y, Pierce DA, Suyama A, Mabuchi K (2012) Studies of mortality of atomic bomb survivors. Report 13: solid cancer and noncancer disease mortality: 1950-1997. Radiat Res 178:AV146–AV172
9. Morgan WF, Bair WJ (2013) Issues in low dose radiation biology: the controversy continues. A perspective. Radiat Res 179:501–510
10. Rothkamm K, Balroop S, Shekhdar J, Fernie P, Goh V (2007) Leukocyte DNA damage after multi-detector row CT: A quantitative biomarker of low-level radiation exposure. Radiology 242:244–251
11. Beels L, Bacher K, Smeets P, Verstraete K, Vral A, Thierens H (2012) Dose-length product of scanners correlates with DNA damage in patients undergoing contrast CT. Eur J Radiol 81:1495–1499
12. Lobrich M, Rief N, Kuhne M et al (2005) In vivo formation and repair of DNA double-strand breaks after computed tomography examinations. Proc Natl Acad Sci U S A 102:8984–8989
13. Kuefner MA, Grudzenski S, Hamann J et al (2010) Effect of CT scan protocols on x-ray-induced DNA double-strand breaks in blood lymphocytes of patients undergoing coronary CT angiography. Eur Radiol 20:2917–2924
14. Rothkamm K, Horn S (2009) gamma-H2AX as protein biomarker for radiation exposure. Ann Ist Super Sanita 45:265–271
15. Rothkamm K, Lobrich M (2003) Evidence for a lack of DNA double-strand break repair in human cells exposed to very low x-ray doses. Proc Natl Acad Sci U S A 100:5057–5062
16. Beels L, Werbrouck J, Thierens H (2010) Dose response and repair kinetics of gamma-H2AX foci induced by in vitro irradiation of whole blood and T-lymphocytes with x- and gamma-radiation. Int J Radiat Biol 86:760–768
17. Beels L, Bacher K, De Wolf D, Werbrouck J, Thierens H (2009) gamma-H2AX foci as a biomarker for patient x-ray exposure in pediatric cardiac catheterization are we underestimating radiation risks? Circulation 120:1903–1909
18. Carroll PD, Nankervis CA, Iams J, Kelleher K (2012) Umbilical cord blood as a replacement source for admission complete blood count in premature infants. J Perinatol 32:97–102
19. Valentin J (2002) Basic anatomical and physiological data for use in radiological protection: reference values: ICRP Publication 89. Ann ICRP 32:1–277
20. Deak P, van Straten M, Shrimpton PC, Zankl M, Kalender WA (2008) Validation of a Monte Carlo tool for patient-specific dose simulations in multi-slide computed tomography. Eur Radiol 18: 759–772
21. Cristy M (1981) Active bone-marrow distribution as a function of age in humans. Phys Med Biol 26:389–400
22. Seuntjens J, Thierens H, Vanderplaetsen A, Segaert O (1987) Conversion factor F for x-ray beam qualities, specified by peak tube potential and HVL value. Phys Med Biol 32:595–603
23. Deak PD, Smal Y, Kalender WA (2010) Multisection CT protocols: sex- and age-specific conversion factors used to determine effective dose from dose-length product. Radiology 257:158–166
24. Council NR (2006) Health risks from exposure to low levels of ionizing radiation: BEIR VII phase 2. The National Academies Press, Washington DC
25. International Commission on Radiological Protection (2007) The 2007 recommendations of the International Commission on Radiological Protection. ICRP publication 103. Ann ICRP 37(2–4)
26. Thomas KE, Wang B (2008) Age-specific effective doses for pediatric MSCT examinations at a large children's hospital using DLP conversion coefficients: a simple estimation method. Pediatr Radiol 38:645–656
27. Miglioretti DL, Johnson E, Williams A et al (2013) The use of computed tomography in pediatrics and the associated radiation exposure and estimated cancer risk. JAMA Pediatr 167:700–707
28. Geisel D, Zimmermann E, Rief M et al (2012) DNA double-strand breaks as potential indicators for the biological effects of ionising radiation exposure from cardiac CT and conventional coronary angiography: a randomised, controlled study. Eur Radiol 22:1641–1650
29. Stephan G, Schneider K, Panzer W, Walsh L, Oestreicher U (2007) Enhanced yield of chromosome aberrations after CT examinations in paediatric patients. Int J Radiat Biol 83:281–287
30. Shrimpton PC, Hillier MC, Lewis MA, Dunn M (2006) National survey of doses from CT in the UK: 2003. Br J Radiol 79:968–980
31. Pages J, Buls N, Osteaux M (2003) CT doses in children: a multicentre study. Br J Radiol 76:803–811
32. Morgan WF (2012) Non-targeted and delayed effects of exposure to ionizing radiation: I. Radiation-induced genomic instability and bystander effects in vitro. Radiat Res 178:AV223–AV236
33. Little JB, Azzam EI, de Toledo SM, Nagasawa H (2005) Characteristics and mechanisms of the bystander response in monolayer cell cultures exposed to very low fluences of alpha particles. Radiat Phys Chem 72:307–313
34. Sokolov MV, Smilenov LB, Hall EJ, Panyutin IG, Bonner WM, Sedelnikova OA (2005) Ionizing radiation induces DNA double-strand breaks in bystander primary human fibroblasts. Oncogene 24:7257–7265
35. Prise KM, O'Sullivan JM (2009) Radiation-induced bystander signalling in cancer therapy. Nat Rev Cancer 9:351–360
36. Azzam EI, de Toledo SM, Little JB (2001) Direct evidence for the participation of gap junction-mediated intercellular communication in the transmission of damage signals from alpha-particle irradiated to nonirradiated cells. Proc Natl Acad Sci U S A 98:473–478
37. El-Saghire H, Thierens H, Monsieurs P, Michaux A, Vandevoorde C, Baatout S (2013) Gene set enrichment analysis highlights different gene expression profiles in whole blood samples X-irradiated with low and high doses. Int J Radiat Biol 89:628–638
38. Mancuso M, Pasquali E, Leonardi S et al (2008) Oncogenic bystander radiation effects in Patched heterozygous mouse cerebellum. Proc Natl Acad Sci U S A 105:12445–12450
39. Jost G, Golfier S, Pietsch H et al (2009) The influence of x-ray contrast agents in computed tomography on the induction of dicentrics and gamma-H2AX foci in lymphocytes of human blood samples. Phys Med Biol 54:6029–6039
40. Brenner D, Doll R, Goodhead D et al (2003) Cancer risks attributable to low doses of ionizing radiation: Assessing what we really know. Proc Natl Acad Sci U S A 100:13761–13766
41. Pernot E, Hall J, Baatout S et al (2012) Ionizing radiation biomarkers for potential use in epidemiological studies. Mutat Res 751:258–286
42. Rübe CE, Grudzenski S, Kühne M et al (2008) DNA double-strand break repair of blood lymphocytes and normal tissues analysed in a preclinical mouse model: implication for radiosensitivity testing. Clin Cancer Res 14:6546–6555
43. Richardson C, Jasin M (2000) Frequent chromosomal translocations induced by DNA double-strand breaks. Nature 405:697–700
44. Khanna KK, Jackson SP (2001) DNA double-strand breaks: signalling, repair and the cancer connection. Nat Genetics 27:247–253
45. Singh S, Kalra MK, Moore MA et al (2009) Dose reduction and compliance with pediatric CT protocols adapted to patient size, clinical indication, and number of prior studies. Radiology 252:200–208